Nanoscale

ROYAL SOCIETY OF CHEMISTRY

MINIREVIEW

View Article Online
View Journal | View Issue

Cite this: *Nanoscale*, 2022, **14**, 17871

Membranes prepared from graphene-based nanomaterials for water purification: a mini-review

Marliyana Aizudin, †[a] Nur Hashimah Alias, †[a] Yun Xin Angel Ng,[a] Muhammad Haikal Mahmod Fadzuli,[a] Seng Chuan Ang,[a] Yi Xun Ng,[a] Rafeeque Poolamuri Pottammel,[b] Fu Yang[c] and Edison Huixiang Ang *[a]

Graphene-based nanomaterials (GBnMs) are currently regarded as a critical building block for the fabrication of membranes for water purification due to their advantageous properties such as easy surface modification of functional groups, adjustable interlayer pore channels for solvent transportation, robust mechanical properties, and superior photothermal capabilities. By combining graphene derivatives with other emerging materials, heteroatom doping and rational design of a three-dimensional network can enhance water transportation and evaporation rates through channels of GBnM laminates and such layered structures have been applied in various water purification technologies. Herein, this mini-review summarizes recent progress in the synthesis of GBnMs and their applications in water treatment technologies, specifically, nanofiltration (NF) and solar desalination (SD). Finally, personal perspectives on the challenges and future directions of this promising nanomaterial are also provided.

Received 27th September 2022,
Accepted 24th November 2022

DOI: 10.1039/d2nr05328d

rsc.li/nanoscale

[a]*Natural Sciences and Science Education, National Institute of Education, Nanyang Technological University, Singapore 637616, Singapore.*
E-mail: edison.ang@nie.edu.sg
[b]*Department of Chemistry, Indian Institute of Science Education and Research Thiruvananthapuram, 695551, India*
[c]*School of Environmental and Chemical Engineering, Jiangsu University of Science and Technology, Zhejiang 212003, China*
†These authors contributed equally.

Introduction

Water is one of the fundamental necessities for the existence of life on Earth. Rapid population growth and depletion of freshwater resources have exacerbated the water scarcity issue. The global water demand is expected to rise by 20–30% from now to 2040, but the conventional water treatment technology

Marliyana Aizudin

Marliyana Binte Aizudin received her MSc in Life Science from the National Institute of Education/Nanyang Technological University and BSc (Hons) degree in Chemistry & Biological Chemistry from Nanyang Technological University. She is currently working as a research assistant (R.A.) under the supervision of Assistant Professor Edison Huixiang Ang. Her current research interests include membrane technology, solar still desalination applications and energy storage applications.

Nur Hashimah Alias

Nur Hashimah Alias is a senior lecturer at Universiti Teknologi MARA, Malaysia. She received her PhD degree from Universiti Teknologi Malaysia in 2020. She is currently a postdoctoral fellow under the host supervisor Assistant Professor Edison Huixiang Ang at the National Institute of Education/Nanyang Technological University, Singapore. Her postdoctoral fellowship is fully funded by the Singapore Academies South-East Asia Fellowship (SASEAF) Programme by the National Research Foundation (NRF). Her current research interests include the development of functional materials, adsorption, photocatalysis and membrane technology for water/wastewater treatment and gas separation.

using distillation is consume high energy and is incapable of producing fresh water to meet the global demand.[1] Due to the high energy cost of producing freshwater *via* distillation, alternative methods such as membrane filtration are preferred because of their low energy consumption, which is nearly 500 times lower than that of the former. Among the different types of membrane filtration techniques, nanofiltration (NF) is the most appealing due to its beneficial advantages of both lower energy cost (compared to reverse osmosis (RO)) and higher water quality (compared to ultrafiltration (UF)).[2] To reduce the carbon footprint of freshwater production, solar desalination (SD) is one of the most attractive sustainable technologies due to its ability to utilize renewable solar energy from the sun to convert light energy into heat energy for desalination.[3–6] Despite the above-mentioned advantages of NF and SD technologies over traditional distillation, the commercial polymeric membrane in NF has limited water permeance,[7,8] while the commercial carbonized solar absorber has poor photothermal conversion efficiency (PTCE).[9] These limitations on materials and design choices restrict the optimal freshwater production rate of the respective technologies. Consequently, a breakthrough in membrane development is required to address the water challenges of the twenty-first century. Two-dimensional (2D) graphene-based nanomaterials (GBnMs) possess a single atom thick sheet with a high specific surface area, strong mechanical properties and broadband light absorption, and can act as building blocks for membrane fabrication, forming interlayer channels for water transportation.[10–12] Recently, there have been several excellent reviews comparing the performances of GBnMs in gas separation,[13] photocatalysis,[14,15] thermal storage,[16–19] biosensors,[20–22] and energy storage.[11] However, a focused review of the synthesis, properties, and performance results of GBnMs for promising water purification applications, particularly NF and SD, is still lacking in the literature.

In this mini-review, we begin by providing a comparison of the characteristics of NF and SD applications, as summarized in Table 1. This is accompanied by a comprehensive overview of recent progress towards the development of emerging membranes of GBnMs comprising graphene derivatives, chemically doped graphene, and graphene-based composites in NF and SD (Fig. 1a). To illustrate the merits of GBnMs, a figure of merit among various membrane materials namely, graphitic, non-graphitic (*i.e.*, coal and activated carbon), inorganic, and commercial membranes in NF is shown in Fig. 1b along with its upper-bound NF performance graphs (Fig. 1c). A similar illustration is also applied to SD applications (Fig. 1d and e). The synthesis methods of GBnMs and their property–performance correlations are reviewed first, followed by a detailed discussion of recent representative articles on NF and SD applications of GBnMs. Finally, personal insights into the critical challenges and future research directions of this interesting research field as solutions towards water purification will be articulated in the later sections.

Synthesis and properties of GBnM membranes

The GBnM membrane is composed of graphene-based nanosheets stacked into a layered structure and deposited on a porous substrate to enable the selective separation of water molecules.[25] This can be carried out *via* vacuum filtration,[26] interfacial polymerization,[27] phase inversion,[28] and so on. The graphene derivatives are categorised into graphene oxide (GO), and reduced GO (rGO). Typically, GO nanosheets can be obtained *via* chemical exfoliation of graphite through Brodie's,[29] Staudenmaier's, or Hummers',[29,30] methods. Then the as-fabricated GO nanosheets can be further reduced into rGO nanosheets *via* electrochemical reduction,[31] microwave reduction,[32] photo-ultrasonic assisted reduction,[33] *etc*. When compared to the rGO-based laminate, the GO-based membrane can facilitate fast water transportation but its rejection rate for a small probe solute is compromised due to its

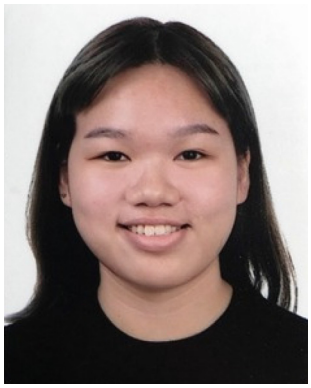

Yun Xin Angel Ng

Ng Yun Xin Angel is currently a final year graduate taking a BSc (Hons) in Chemistry and Biological Chemistry in Nanyang Technological University (NTUSG). She previously undertook research at the National Institute of Education (NIE) under the supervision of Assistant Professor Edison Huixiang Ang. She worked on the production and electrical testing of zinc-ion batteries (ZIB) and experimented the use of gelatine-based electrolytes.

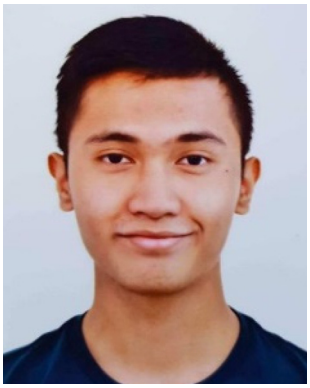

Muhammad Haikal Mahmod Fadzuli

Muhammad Haikal Bin Mahmod Fadzuli graduated from Nanyang Technological University with a BSc (Hons) in Chemistry and Biological Chemistry as well as a minor in Environmental Sustainability in 2021. During his undergraduate studies, he interned at the National Institute of Education (NIE) under the supervision of Assistant Professor Edison Huixiang Ang. During his time there, his main research studies were focused on polymeric membranes for wastewater treatment and the synthesis of graphene-based inks for 3D printing for use in the membrane projects.

Table 1 Comparison of the characteristics of NF against SD processes in terms of 5-star rating[23,24]

Process	Mechanism	Lifespan	Energy consumption (kW h)	Water production rate (L h^{-1})	Cost per litre ($ per L)
Nanofiltration	(1) Physical adsorption (2) Size exclusion (3) Donnan effect	★★★★☆	★★★★☆	★★★★☆	★★★☆☆
Solar desalination	(1) Plasmonic localized heating (2) Electron hole generation and relaxation (3) Thermal vibration	★★★☆☆	★☆☆☆☆	★★☆☆☆	★★☆☆☆

e.g. ★★★★★ = high, ★☆☆☆☆ = low.

enlarged interlayer channels in the NF field with the same thickness as that of the graphene derivative-based membrane.[34] For SD application, rGO membranes are more well-studied over the GO membrane due to their excellent photothermal conversion properties.[35] Several studies have shown that chemically doping nitrogen into the graphene derivatives can further improve the water production rate of the GBnM membrane in both NF[36] and SD.[37] Nitrogen has a comparable atomic size to carbon, making it suitable for doping, and nitrogen (N) doping can also increase the hydrogen binding sites on the rGO or GO to promote excellent wetting ability with water molecules, resulting in fast water permeation through the N-doped graphene laminates.[38] In a typical synthesis of N-doped graphene materials, a nitrogen source (*i.e.*, melamine[39] or ethylenediamine[38]) is used and thermal treatment at a higher temperature (*i.e.*, 200 °C *versus* 1000 °C) can increase the N-doping effect, which in turn improves the hydrophilicity of the N-doped graphene laminates.[38] The graphene derivatives can also be added to other emerging materials, such as transition metal oxides (TMO),[40] transition metal dichalcogenides (TMD),[41,42] carbon nanotubes (CNT),[43–46] polymers,[47–49] zeolites,[50,51] *etc.*, forming graphene-based composites. Due to their excellent chemical stability, increased specific surface area, tuneable surface charge and interlayer channels as well as enhanced photothermal efficiency, such graphene-based composite membranes can further improve the water production rates and separation performances of the membrane technologies. The practical utilization of GBnM membranes for NF and SD applications is discussed in detail in the following section.

GBnM membranes for NF

NF for GBnM membranes is typically governed by the following separation mechanisms:[52,53] (1) physical adsorption or chemical interaction (*i.e.*, cation–π interaction) between solute molecules and the surfaces of mass transport channels, (2) molecular sieving controlled by size exclusion, and (3) the Gibbs–Donnan effect (*i.e.*, electrostatic repulsion) between charged solutes and charged groups anchored to the membrane surface. These mechanisms are interconnected, and the last two modes are more important in NF processes.[8] A GBnM selective layer is normally supported on a microporous UF support in the GBnM NF membrane. In NF, the following two parameters are important to evaluate the separation performances of the NF membrane and the permeance (F), which can be determined using eqn (1):[54]

$$F = \frac{V_p}{A \times t \times \Delta P} \quad (1)$$

where V_P is the permeate volume (L), A is the effective area of the membrane (m^2), t is the permeation time, and ΔP is the operating pressure. Therefore, the unit of F is L m^{-2} h^{-1} bar^{-1}.

Seng Chuan Ang

Seng Chuan Ang graduated from Nanyang Technological University (NTU) with a BSc (Hons) in Pure Physics with concentration on Nanotechnology in 2021. During his internship at the National Institute of Education (NIE), he was under the supervision of Assistant Professor Edison Huixiang Ang. His research was mainly focused on the construction of solar evaporator systems and the optimization of nanocarbon surfaces in addition to the synthesis of plastic waste to produce new nanocarbon surface combinations.

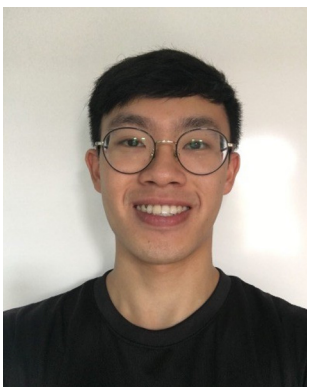

Yi Xun Ng

Yi Xun Ng is currently a final year undergraduate studying in Nanyang Technological University (NTU), with a major in Physics. Currently undertaking internship at the National Institute of Education (NIE) under the supervision of Assistant Professor Edison Huixiang Ang, his current research and experimental work entail the production and electrical testing of zinc-ion batteries (ZIBs). Other works include membrane filtration technology and synthesis of materials such as processing plastic into carbon black powder.

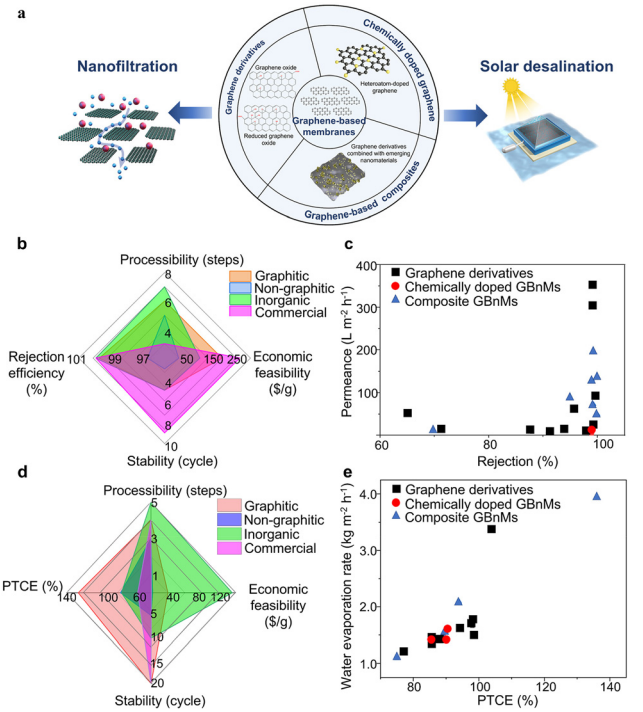

Fig. 1 (a) Schematic illustration of membranes prepared from graphene derivatives, chemically doped graphene, and graphene-based composites for NF and SD applications. Figure of merit comparing processibility, economic feasibility, stability, and performance factors of (b) NF among various membrane materials and (c) upper-bound graph of NF. Figure of merit comparing processibility, economic feasibility, stability, and performance of (d) SD among various membrane materials and (e) upper bound graph of SD.

The rejection percentage (R%) of the probe solute can be determined using eqn (2):[7]

$$R = \frac{C_F - C_P}{C_F} \times 100\% \quad (2)$$

where C_F is the concentration of the feed solution and C_P is the concentration of the permeate.

With regard to the recent progress of the separation performances in NF, the different classes of GBnM membranes which comprise graphene derivatives, chemically doped graphene, and graphene-based composites are summarised in Table 2 and discussed in detail below.

Graphene derivative-based NF membranes

As is known, graphene derivates are categorized into two main classes, GO and rGO. GO-based membranes are rich in oxygenated-functional groups such as carboxyl, carbonyl, epoxy, hydroxyl, and lactol groups.[55] This results in high-water permeability.[56] Marjani *et al.* have developed a GO laminate structure supported on a porous polyethersulfone (PES) substrate, namely the GO/PES membrane, using Hummers' method to fabricate the GO followed by phase inversion to make the NF membrane for water purification.[57] Probe solutes such as methylene blue (MB) and methyl orange (MO) are used to simulate the waste in the wastewater. Upon filtration, the rejection rates of the GO/PES membrane are ~70% and ~88%, respectively, with a relatively high permeance of ~5 to 8 L m^{-2} h^{-1} bar^{-1} due to the high hydrophilicity of the membrane verified by contact angle measurement. In another similar work, Li *et al.* improved the stability of the GO layers on the UF support (polyamide, PA) by a nucleophilic substitution strategy to react the hydroxyl groups of GO with the chloromethyl groups of chloromethylated polysulfone, resulting in polysulfone (PSf)-grafted GO that was anchored to the PA substrate.[58] Such rational design not only improved the mechanical strength of the membrane against shear force, but also enlarged the interlayer for fast water transportation at a permeance range of 25.9–88.0 L m^{-2} h^{-1} bar^{-1} with a rejection rate above 90% for probe solutes like acid black 1 (AB1), Congo red (CR) and MB. Despite the high water production rate of GO-based membranes, the rejection rate still cannot sustain

Rafeeque Poolamuri Pottammel

Rafeeque Poolamuri Pottammel is a scientific illustrator. He works with researchers, developing scientific illustrations for scientific publications and science communication projects. He completed his BS-MS dual degree with a major in Chemistry from IISER Thiruvananthapuram (IISER TVM) in 2016 and has been working on scientific illustration and animation projects for the past 5 years at IISER TVM and IISER Pune. He is also the founder of 'Scidart Academy', an online learning platform for scientists to learn graphic design for science communication.

Fu Yang

Fu Yang received his PhD from Nanjing Tech University working with Prof. Yan Kong. During this period, he also worked with Prof. Ning Yan at the National University of Singapore (NUS) as a China Scholarship Council (CSC) exchange student. He is currently an associate professor at the Jiangsu University of Science and Technology. His research focuses on molecular sieve catalysts and nanostructure functional composite materials specific to heterogeneous selective catalytic reaction and adsorption separation of gas.

the filtration process for long due to the swelling effect of the GO laminate in water.[59]

To overcome the swelling effect of GO membranes, rGO has become appealing because, after reducing GO to rGO on the microporous support, the rGO nanosheets are held strongly by π–π interaction, resulting in the swelling of the NF membrane being minimized.[60] For instance, Li *et al.*[26] reported the fabrication of rGO on a PES support *via* vacuum filtration followed by a heat treatment process. Through the annealing studies at various temperatures, it has been observed that after thermally treating the rGO/PES membrane at 80 °C *versus* 150 °C, the water permeance of the higher temperature treated membrane shows a significant drop in permeance from 7.3 to 3.9 L m^{-2} h^{-1} bar^{-1} and the Na_2SO_4 rejection increases from 57.7% to 90.9% due to the narrowing of the laminar channels after GO has been reduced into rGO at the higher annealing temperature. Although, the rejection percentage of small salt ions is excellent, the permeance of rGO/PES has been compromised in this case. To remedy this issue, Fan *et al.*[61] have created structural defects on the rGO laminate supported on polyvinylidene fluoride (PVDF) by a hydrothermal treatment followed by vacuum filtration. Based on this study, the reaction time of hydrothermal treatment plays an important role in creating defects on the rGO/PVDF membrane and the optimum defects obtained are at the reaction time of 6 h. The number of defects increases when the reaction time increases from 0 to 6 h, as verified by Raman measurement based on the D band presence in the as prepared rGO. Once the reaction time exceeds 6 h, more sp^2 carbon are formed, represented by the G band of the Raman analysis, resulting in a smoother rGO layered structure on the PVDF support, as confirmed by scanning electron microscopy (SEM), which showed a decrease in the number of wrinkles. The defect rich rGO/PVDF membrane at 6 h of reaction time has an optimal separation performance at 20 L m^{-2} h^{-1} bar^{-1} with a rejection rate of 99% for MB. To improve the affinity of the GO laminates on the PES support, the GO nanosheets were first functionalized using 3-aminopropyltriethoxysilane (APTS) followed by non-solvent induced phase inversion onto the PES support while polyvinylpyrrolidone (PVP) was used to create pores on the membrane.[62] The resultant APTS functionalized GO/PVP-PES membrane showed a high permeance of 53.8 L m^{-2} h^{-1} bar^{-1} with rejection rates of 65.3% and 14.6% for sunset yellow (SY) and $MgSO_4$, respectively. To tune the interlayer channel spacing of the NF membrane, Xing *et al.*[63] introduced chitosan into the GO laminate, which was filtered onto electrospun polyacrylonitrile (PAN) and by increasing the GO/chitosan ratio from 1 : 50 to 1 : 125, the rejection rate of Direct Red 80 (DR 80) improved from 78% to >99%, while obtaining a maximum permeance of 351.6 L m^{-2} h^{-1} bar^{-1}. This indicates that chitosan can help to regulate the pore-size channels of the GO membrane. Unfortunately, the salt rejection for such GO membrane was still low at 1.3 to 4.6% for Na_2SO_4. To resolve the low salt rejection rate, Liu *et al.*[67] used a rod coating method to uniformly coat GO onto PA support, after which, UV irradiation was used to reduce the GO into rGO, leading to a reduction of interlayer spacing, and thus the rejection rate of Na_2SO_4 enhanced significantly to 96%. Apart from 2D GO nanostructures, 0D GO quantum dots (GOQDs) on PA supported have also been reported for NF.[68] It has also been demonstrated that the GOQD/PA membrane displayed a relatively high water permeance of 10.9 L m^{-2} h^{-1} bar^{-1} but a low rejection of 71% for MB. To improve the rejection rates of dyes as well as the water permeance, Cho *et al.*[69] embedded GO nanoribbons (GONRs) into the rGO laminates and deposited them onto a nylon support *via* vacuum filtration. In such a configuration, the nanochannels can be enlarged without compromising the stacking of rGO layers, resulting in a high water permeance from 185.3 to 301.9 L m^{-2} h^{-1} bar^{-1} with rejection rates more than 95% for methyl red (MR), MO, MB, and Rose Bengal (RB).

Chemically doped graphene-based membranes

To date, nitrogen is one of the most common dopants used due to its similar atomic size to carbon and nitrogen doping can also increase the hydrogen binding sites on the rGO or GO to promote excellent wetting ability with water molecules, leading to rapid water permeation through the N-doped graphene laminates.[38] Recently, García-Picazo *et al.*[27] have reported a NF membrane that consists of N-doped GO selective layer supported PA ultrafilter. The GO was first prepared from graphite using the Marcano–Tour approach with modification, then ethylenediamine and 1-[bis(dimethylamino)methylene]-1*H*-1,2,3-triazolo[4,5-*b*]pyridinium 3-oxide hexafluoro-phosphate were added as a solvent/N-dopant and nitrogen co-dopant, respectively, for solvothermal treatment and finally, the interfacial polymerization method was employed to obtain the N-GO/PA membrane. A similar method was used to prepare an undoped GO/PA membrane as a control experiment. In this study, it has been demonstrated that the water permeance increases from 1.1 to 1.9 L m^{-2} h^{-1} bar^{-1} and the salt rejection of Na_2SO_4 increases from 95.9% to 98.9% and that of NaCl increases from 46.2% to 61.7% at 2000 ppm, after

Edison Huixiang Ang

Edison Huixiang Ang is currently an assistant professor at the National Institute of Education/Nanyang Technological University. He is also an Early Editorial Board Member of Chemical Engineering Journal, *Editorial Board Member of* Scientific Reports, *and Associate Editor of* Frontiers in Chemistry. *His current research interests combine nanotechnology, 2D nanomaterials and additive manufacturing approaches to develop functional nanostructures for advanced energy storage, membrane technology, catalysis, and sensing applications.*

Table 2 Summary of GBnM membranes in NF

GBnM membranes	Fabrication method	Permeation ($L\ m^{-2}\ h^{-1}\ bar^{-1}$)	Rejection or selectivity	Ref.
Graphene derivative-based membranes				
GO/PES	Hummers' method + phase inversion	~5 to 8	Methylene blue: ~70, methyl orange: ~88	57
GO-PSf/PA	Nucleophilic substitution reaction + vacuum filtration	25.9 to 88.0	Acid black 1: 90.3; congo red: 99.5; methyl blue: 99.8	64
rGO/PES	Vacuum filtration + heat treatment	3.99	Na_2SO_4: 90.9	26
rGO/PVDF	Hydrothermal treatment + vacuum filtration	20	Methyl blue: 99	61
APTS functionalized GO/PVP-PES	Hummers' method + APTS functionalization + non-solvent induced phase inversion	53.8	Sunset yellow: 65.3; $MgSO_4$: 14.6	65
Chitosan modified GO/PAN	Ultrasonication + vacuum filtration	235.5 to 351.6 78.5 to 117.2	Direct red 80: >99; Na_2SO_4: 1.3 to 4.6	66
Ultrathin rGO/PA	Hummers' method + sonication + mechanical stirring + rod-coating + UV reduction	60.0	Na_2SO_4: 96	67
GO quantum dots/PA	Ultrasonication + pressure-assisted filtration	10.9	Methylene blue: 71	68
rGO–GO nanoribbons/nylon	Ultrasonication + vacuum filtration	211.2 301.9 185.3 245.1	Methyl red: >99; methyl orange: 95.3; methylene blue: 96.3; rose bengal: >99	69
Surface modified GO	Hummers' method + pressure-assisted filtration-deposition + dip-coating	10.5	$MgCl_2$: 93.2; Na_2SO_4: 93.9	70
GO–PDA/O═CS/ceramic	Dip-coating	11.8	Dye: 98.3	71
GO/PEI/PAN	Spin coating	0.43	K^+: 33.8; Mg^{2+}: 33.8	72
Chemically doped graphene-based membranes				
N-doped GO/PA	Marcano-Tour method + solvothermal treatment + interfacial polymerization	1.9	Na_2SO_4: 98.9; NaCl: 61.7	27
N-doped graphene and GO hybrid/PVDF	Ultrasonication + vacuum filtration	6.13	Eriochrome black T: 99; crystal violet: 99; trypan blue: 99; neutral red: 98; methylene blue: 98	36
Graphene-based composite membranes				
ZIF-8@f-GO/ceramic	Pressure filtration + freeze drying + *in situ* growth	49.8	Methylene blue: ~100	73
ZIF-8-GO/CA	Mechanical stirring + vacuum filtration	136.4	Methylene blue: ~100	74
COF–TiO_2@GO/PAN	Nonsolvent induced phase-separation + interfacial polymerization	89.0	Congo red: 94.8	75
2D COF–prGO 0.3/nylon	Sonication + chemical reduction + pressure filtration	194	Methylene blue: >98; acid orange 7: >98; rhodamine B: >98; methyl orange: >99.3	76
SiO_2–SGO-0.3/PES	Hummers' method + ultrasonication + vacuum filtration	72.8	Methyl orange: 99.3	77
PEI modified GO–MXene/PVDF	Ultrasonication + vacuum filtration + PEI soaking	9.5	Ca^{2+}: >70; Mg^{2+}: >70	78
PEI modified GO/nylon	Mechanical stirring + vacuum filtration	131.1 131.1	Direct red: >99; methyl blue: >99	79

N-doping was applied on the pristine GO. In another similar work, Hou *et al.*[36] uses N-doped graphene mixed with GO to synergistically improve both the permeance and rejection rate of NF membranes. The N-doped graphene was first mixed with GO *via* ultrasonication followed by vacuum filtration onto PVDF to obtain the N-doped graphene–GO/PVDF membrane. Different mass ratios of GO and N-doped graphene (*i.e.*, 1 : 0, 3 : 1, 1 : 1 and 0 : 1) were employed on the membrane to evaluate the NF performances. In this study, it was shown that the addition of N-doped graphene nanosheets into the membrane reduces the water contact angle of the GO membrane and this observation contradicted the previous study. However, it has been shown that the introduction of N-doped graphene nanosheets into GO nanosheets can reduce the interlayer spacing as verified by the X-ray diffraction (XRD) patterns. This might be because the intercalated N-doped graphene in GO laminates has developed more π–π interactions, causing the channel width to narrow. Because of this, the rejection rates will increase while the permeance is compromised. The optimized mass ratio of GO and N-doped graphene was reported to be 3 : 1 where the N-doped graphene-GO/PVDF membrane exhibited a permeance of 6.13 $L\ m^{-2}\ h^{-1}\ bar^{-1}$ with rejection rates of near 99% for probe solutes, eriochrome black T (EBT), crystal violet (CV), trypan blue (TB), neutral red (NR), and MB. However, clear scientific mechanisms of other chemically doped graphene are still under investigation and their groundbreaking studies are expected in the near future.

Graphene-based composite membranes

The combination of graphene derivatives and other emerging nanomaterials often results in a synergistic effect in both water production rate and quality of the water when compared to its pristine form. For example, Zhang *et al.*[73] have coated GO laminates onto the ceramic support *via* pressure filtration then applied freeze drying to remove water molecules followed by *in situ* crystallization growth of ZIF-8 nanocrystals to facilitate the enlargement of the interlayer spacing of microporous defects and improvement in the mechanical property of the membrane. The resultant ZIF-8@f-GO/ceramic membrane has a thickness of 103 nm, and when compared with the GO membrane (GOm) and freeze-dried GO membrane (f-GOm), the ZIF-8@f-GOm showed a higher water permeance of ~60 L m^{-2} h^{-1} bar^{-1} (30-fold higher than GOm) without much decay of permeance after 180 h of prolonged filtration, indicating the robust stability of the hybrid membrane. In another similar work, Qu *et al.*[74] studied the different sizes of ZIF-8 nanocrystals (*i.e.*, 35, 60, 100, 150 nm) and they observed that the optimal separation performance is attained by the NF membrane embedded with 100 nm sized ZIF-8 nanocrystals. The as-prepared ZIF-8–GO composite was deposited onto cellulose acetate (CA) support *via* vacuum filtration, and it showed a superior permeance of 136.4 L m^{-2} h^{-1} bar^{-1} (6 times higher than that of pristine GO membrane) with near perfect rejection for MB. This shows that by introducing different sizes of ZIF-8 cross-linkers, the nanochannel width of the laminates can be altered to improve the molecular separation performances of the NF membrane. This observation is in agreement with another reported study of metal organic framework (MOF) membranes using polycation cross-linkers.[53] Covalent organic frameworks (COF), like MOF, have a periodic pore system which makes them appealing for use in molecular separation processes. For instance, Liu *et al.*[75] have fabricated TiO_2@GO supported on PAN support *via* nonsolvent induced phase-separation (NIPS) followed by the addition of a 1,3,5-triformylphloroglucinol–*p*-phenylenediamine (TpPa)-based COF composite layer using interfacial polymerization (IP) methods, as shown in Fig. 2a. During the NIPS process, synergistic effects between GO nanosheets and TiO_2 nanoparticles result in the self-migration of TiO_2@GO nanoparticles to the top surface and pore walls of the PAN membranes, where they formed more homogeneous hydrophilic diffusion channels, hydrophilic top surface and highly ordered COF layer as shown in Fig. 2b. On top of that, the calculated mean pore size of the TpPa/TiO_2@GO/PAN membrane's top surface from filtration data (1.78 nm) was found to be higher as compared to that of other prepared membranes and is consistent with pore size measurements from N_2-adsorption experiment (1.80 nm), and theoretical value calculated from the molecular structure (1.83 nm), confirms a single crystal with ordered pore structures of TpPa/TiO_2@GO/PAN membranes. Due to this reason, this composite membrane exhibited a relatively higher water permeance of 89.0 L m^{-2} h^{-1} bar^{-1}. Meanwhile, the CR solution permeance decreased from 38.7 to 28.7 L m^{-2} h^{-1} bar^{-1} after the first 18 h, then remained stable up to 282 h. However, the CR rejection rate increased slightly from 97.5% to 98.5%, then remained constant at 99%, as shown in Fig. 2c.

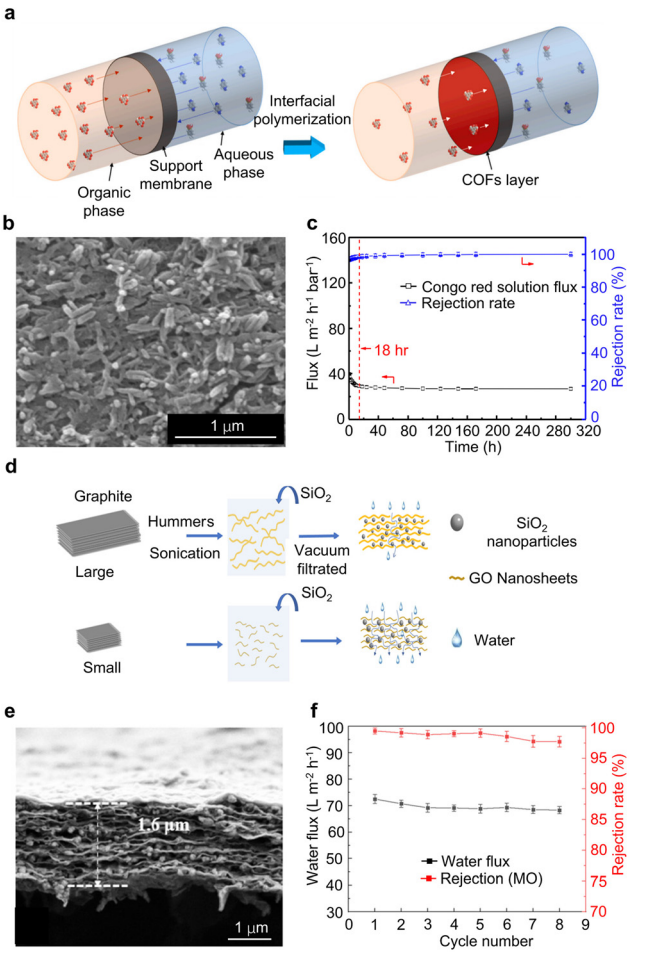

Fig. 2 (a) A schematic illustration of the COF composite membrane *via* interfacial polymerization. (b) FESEM image of COF layer and (c) CR probe solute filtration performance of COF composite membrane.[75] This figure has been adapted from ref. 75 with permission from Elsevier, Copyright 2022. (d) Schematic illustration of GO/SiO_2 composite membrane fabrication with various laminate sizes. (e) Cross-sectional SEM image GO/SiO_2-30. (f) Long-term stability measurement for GO/SiO_2-30 membrane filtration using MO probe solute.[77] These figures have been adapted from ref. 77 with permission from Elsevier, Copyright 2022.

In another similar study, Sui *et al.*[76] have used a 2D COF in combination with partial rGO for NF and this composite membrane was fabricated by mixing the as-prepared 2D COF and GO nanosheets then reducing the GO into rGO using L-ascorbic acid and lastly using pressure filtration onto a nylon support to obtain the 2D COF–prGO-0.3/nylon membrane. In this study, the optimal mass ratio composition of COF : prGO was investigated and found to be 0.3, which gave rise to a permeance of 194 L m^{-2} h^{-1} that was 27 times higher than that of the pristine prGO membrane with similar rejection rates of >98% for organic dyes (*i.e.*, MB). Such a high permeance was due to the 2D COF nanosheet reinforced prGO laminates,

resulting in self-supporting structures with numerous wrinkles and corrugations above large pores. As a result, the effective membrane surface area increased by 53.4%, leading to an enhancement of the water permeance. In another study, Deng *et al.*[77] have investigated the size effects of a GO nanosheet (*i.e.*, SGO: 0.4–1.2 μm, MGO: 2.0–6.2 μm, and LGO 17–23 μm) hybrid with SiO_2 nanoparticles (25 nm in diameter) on the molecular separation for NF. Different sizes of GO were fabricated from various sizes of graphite flakes *via* the Hummers' method, then the GO nanosheets were mixed with SiO_2 nanoparticles by ultrasonication and lastly the COF was coated on this hybrid supported on PES by the vacuum filtration method (see Fig. 2d). As shown in Fig. 2e, the cross-sectional SEM image GO/SiO_2 shows a GO nanosheet assembly intercalated with SiO_2 nanoparticles, in which the thickness of the composite increased up to 1.6 μm. For this reason, the SGO membrane with an optimal mass ratio of SiO_2 : SGO as 0.3 demonstrated the highest water flux of 72.8 L m^{-2} h^{-1} under 1 bar with a comparable rejection rate (>99%) for MO (see Fig. 2f). These results showed that a small GO nanosheet assembly with intercalated SiO_2 nanoparticles could create plentiful nanochannels by introducing pores for fast water permeation without compromising the rejection rate.

Other classes of nanomaterials such as 2D MXene nanosheets have also been coupled with GO nanosheets into membranes for NF. For example, Zhao *et al.*[78] mixed GO and MXene nanosheet dispersions *via* ultrasonication with an optimal mass ratio of 1 : 4 and then deposited the mixture onto the PVDF support *via* vacuum filtration followed by soaking in a solution containing polyethylenimine (PEI), forming the PEI modified GO-MXene/PVDF membrane (see Fig. 3a). The PEI modified GO/MXene membrane has a positively charged surface as indicated by the zeta potential measurement due to the large amounts of PEI that is attached to the top surface (Fig. 3b) when compared to the pristine GO and the GO/MXene membranes. This composite membrane exhibited a water permeance of 9.5 L m^{-2} h^{-1} with >70% rejection for Ca^{2+} and Mg^{2+} (Fig. 3c), which is 7 times higher compared to that of the GO membrane. The arrangement of the layered structure of the composite membrane which results in a high rejection rate towards positively charged probe solutes is due to the Donnan effect in the presence of polycations (*i.e.*, PEI). On top of that, according to Huang *et al.*,[80] PEI not only controls the charge property of the interlayer channels but also increases the hydrophilicity of the membrane surface, resulting in enhanced water permeance. They have previously tuned the interlayer of negatively charged GO layers using positively charged PEI *via* layer-by-layer assembly for the coating of PEI and GO was employed on the PAN substrate to improve the bonding between GO and the substrate (Fig. 3d). They optimized the interlayer channel structure while regulating the charge attraction between PEI and GO and made the stack of GO nanosheets flatter, thus enhancing the smoothness of the GO–PEI membrane surface. As seen from Fig. 3e, the 15-bilayer membrane showed no obvious interface of each layer due to the enhanced electrostatic attraction enabled by

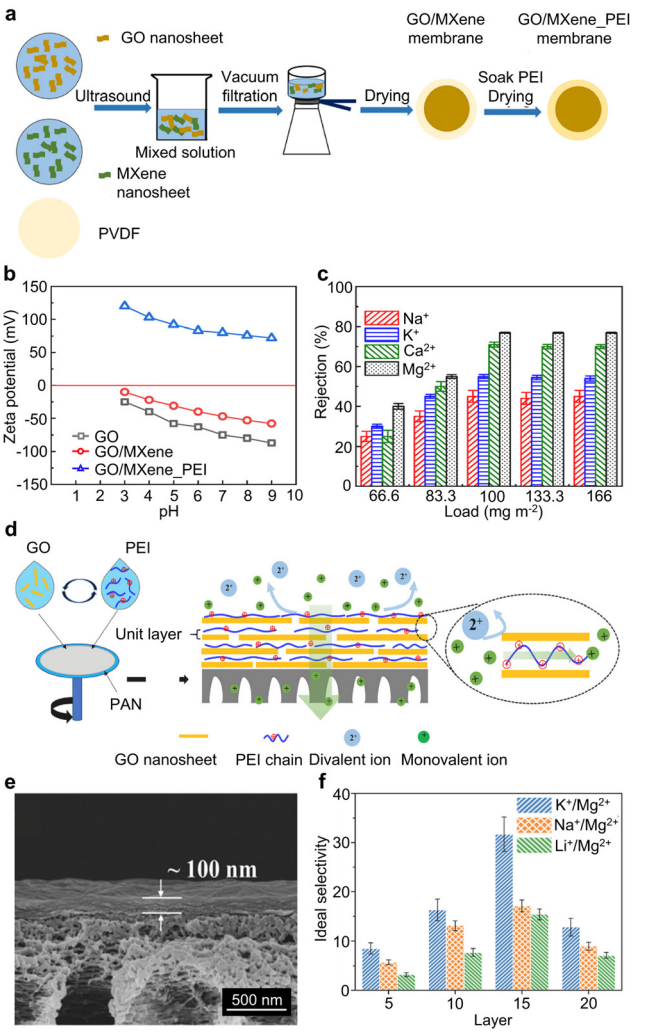

Fig. 3 (a) Schematic illustration of PEI modified GO-MXene/PVDF membrane preparation. (b) Zeta potential of various membranes at pH 3–9. (c) Ion rejection membrane of GO/MXene_PEI membrane with different loadings.[78] These figures have been adapted from ref. 78 with permission from the Elsevier, Copyright 2021. (d) Fabrication of GO-PEI membrane and its mono/divalent ion transport pathways. (e) SEM image of the cross-section of GO-PEI membrane with 15 bilayers. (f) Effect of the number of GO-PEI bilayers on the membrane separation performance of mono-/divalent ions (PEI concentration is 0.05 wt%).[80] These figures have been adapted from ref. 80 with permission from the Elsevier, Copyright 2022.

PEI intercalation. The addition of PEI increased the membrane thickness by hindering the volatilization of the residual water within the membrane interlayer. The 15 bilayer GO–PEI membrane also exhibited optimal mono-/di-valent ion separation performance, with perm-selectivity of K^+/Mg^{2+}, Na^+/Mg^{2+}, and Li^+/Mg^{2+} of 31.7, 17.1 and 15.4, respectively, as shown in Fig. 3f. As the PEI concentration increases, the positive charges in the GO–PEI membrane also increase and cause the ion permeation rates to decrease due to the increase in charge repulsion. Thus, the divalent ions experienced a stronger repulsive force and led to the gradual increase of the perm-selectivity of mono-/di-valent ions to gradually increase.

On the other hand, Zhang *et al.*[81] had previously firmly adhered GO laminate onto the substrate by synergistically coupling the chemical Schiff base reaction and physical van der Waals interactions. As a result, the separation performance and stability in water of the as-prepared GO-PDA/O=CS/MCE membranes exhibited a water permeance of 8.1 L m^{-2} h^{-1} bar^{-1} with a remarkable dye rejection of 98.3%. This excellent performance resulted from the molecule-bridged GO membrane featuring superior stability in a robust separation environment. Moreover, the as-prepared membrane also possessed excellent durability in crossflow filtration, high-pressure, and prolonged filtration, and the ability to withstand vibration and sonication treatment. In another work by Zhang *et al.*,[82] they manipulated the membrane surface charge to control ion transport through GO membranes. In this work, the ionizable functional groups with various protonation/deprotonation capacities on the surface of GO laminates were successfully created and finely tailored. As a result, the resulting membrane exhibited excellent salt retention capability with a water permeance of ~10.5 L m^{-2} h^{-1} bar^{-1} and $MgCl_2$ rejection of ~90%. During filtration, the highly charged surface of the GO membrane repels high-valent co-ions. Furthermore, the high filtration performance is also assisted by a high interaction energy barrier while concomitantly restraining permeation of electrostatically attracted low-valent counterions in an overall balanced solution charge.

To study the effects of different molecular weights of PEI (*i.e.*, 600 and 10 000 kDA), Lu *et al.*[79] prepared a PEI–GO composite by the mechanical stirring of PEI and GO dispersions then vacuum filtration onto a nylon support. It has been demonstrated that when a higher molecular weight of PEI was used to make the PEI(10 000)–GO/nylon membrane, the water permeance was almost 2 times higher than that of PEI(600)–GO/nylon membrane and 20 times higher than that of the pristine GO membrane with similar rejection rates (>99%). This enhanced water permeance of the PEI(10 000)–GO/nylon membrane is due to the enlarged interlayer spacing of the GO layered by the grafting PEI.

GBnM membranes for SD

Solar-powered water evaporation is an environmentally friendly and sustainable method of water desalination.[83] Typically, the photothermal membrane comprises a solar absorber (*i.e.*, GBnM) and a porous substrate. In general, the key properties required for making a photothermal membrane for SD are as follows: (1) wide broadband solar light absorption of photothermal layer; (2) fast water transportation through the 2D laminates; and (3) high photothermal conversion efficiency (PTCE) of the photothermal membrane. The following three parameters are important to evaluate the performances of the photothermal membrane. The water evaporation rate parameter can be calculated according to the following eqn (3):[84]

$$m = \frac{\Delta m}{S \times t} \quad (3)$$

Where Δm refers to the mass change of water (kg), S refers to the area of the photothermal membrane (m^2), and t refers to the solar illumination time (h). Therefore, the unit of m is kg m^{-2} h^{-1}.

The PTCE (%) of the photothermal membrane can be computed using eqn (4):[84]

$$\mathrm{PTCE} = \frac{m' \times h_{\mathrm{LV}}}{P_{\mathrm{in}}} \quad (4)$$

where m' is the water evaporation rate of the solar absorber after subtracting the water evaporation rate of simulated seawater in the dark, h_{Lv} is the latent heat for vaporization of water which is normally taken to be 2.26 kJ g^{-1} in the region of interest, and P_{in} is the incident solar power at 1 kW m^{-2} (= one-sun illumination).

The rejection percentage (R%) computation is similar to that of eqn (2),[85] where C_{F} is the concentration of the metal ion/dye in the original solution and C_{P} is the concentration of the remaining metal ion present after SD.

In terms of recent advancements in SD separation performance, the various classes of GBnM membranes comprising graphene derivatives, chemically doped graphene, and graphene-based composites are summarized in Table 3 under one-sun illumination (1 kW m^{-2}) and discussed in greater detail below.

Graphene derivative-based membranes

Graphene derivatives are particularly appealing for photothermal layer fabrication due to their high specific surface area, broad solar absorption, excellent photothermal capability, and porous interlayer spacing for water transportation.[86] To improve on the characteristics of existing graphene derivative-based membranes, great efforts have been made to develop photothermal membranes with improved photothermal capability and higher water evaporation rates. Taking inspiration from the stable interfacial floatability of lotus leaves, Han *et al.*[85] reported the fabrication of a hydrophobic/hydrophilic bilayer membrane using a laser scribe followed by unilateral oxygen plasma treatment on polyimide (PI) film, producing a laser induced graphene/oxidized laser induced graphene (LIG/LIG-O) membrane. In brief, laser treatment on the one end of the PI film resulted in the formation of a hydrophobic graphitic structure on the LIG side, whereas oxygen plasma treatment on the other end resulted in the formation of hydrophilic oxygen-containing groups on the LIG-O side, forming a hydrophobic/hydrophilic bilayer membrane. The LIG/LIG-O membrane showed a high-water evaporation rate of 1.51 kg m^{-2} h^{-1} with a 77% PTCE, which can be attributed to the combination of microscale capillary water transport, hydrophobic/hydrophilic integrated Janus membrane wettability and nanoscale light trapping. In another work, a photothermal membrane comprising of a rGO solar absorber deposited on filter paper was successfully synthesized firstly by Hummers' method to obtain GO followed by using L-ascorbic acid for mild chemical reduction into rGO and lastly the rGO dispersion was deposited onto filter paper *via* vacuum filtration to produce the rGO/filter paper membrane.[35] Compared to the previous work,

Table 3 Summary of GBnM membranes in SD

GBnM membranes	Fabrication method	Water evaporation rate (kg m^{-2} h^{-1})	PTCE (%)	Selectivity or rejection (%)	Ref.
Graphene derivative-based membranes					
LIG/LIG-O	Laser scribe + O_2 plasma treatment	1.19	77	Na^+: ~100; K^+: ~100; Mg^{2+}: ~100; Ca^{2+}: ~100	85
rGO/filter paper	Hummers' method + chemical reduction + freeze drying + vacuum filtration	1.37	86	—	35
GFs/cellulose fiber paper	Annealing + ethanol deposition + template removal + filtration	1.40	88	Cu^{2+}: 99.9; Mn^{2+}: 99.9; Cd^{2+}: 99	87
rGO/Chitosan modified BHSF	BHSF coated with chitosan + GO coating + chemical reduction	1.43	86	K^+: ~99; Ca^{2+}: ~99; Na^+: ~99; Mg^{2+}: ~99	88
3D rGO–CNCs/MF	Modified Hummers' method + acid hydrolysis + mechanical stirring + squeezing-immersion + chemical reduction	1.66	98	Ca^{2+}: 99.9; K^+: 99.9; Na^+: 99.9; Mg^{2+}: 99.9	89
3D rGO/PBONF aerogel	Molding + freeze drying	1.74	98	-	90
2D g-CNS_{PB}	Solvothermal + carbonization + vacuum filtration	1.50	99	-	91
rGO/CF	Painting + chemical reduction	1.62	94	-	92
V-rGO foam	Freeze drying + chemical reduction	3.39	104	Na^+: 99.9; Mg^{2+}: 99.9; K^+: 99.9; Ca^{2+}: 99.9; B^{3+}: 99.4	93
Chemically doped graphene-based membranes					
N-doped rGO aerogel	Hydrothermal reduction + freeze drying + thermal annealing	1.41	86	-	38
3DN-doped rGO aerogel	Dip-coating + air-drying + thermal annealing	1.56	90	-	39
N-doped graphene quantum dot hydrogel	Hydrothermal treatment + self-assembly reduction	1.40	90	-	37
Graphene-based composite membranes					
g-C_3N_4/GO hybrid hydrogel	Mechanical stirring + hydrothermal treatment	1.09	75	Na^+: ~99.9	94
Cu@G/CLS	Hydrothermal treatment + pyrolysis	1.54	90	Methylene blue: ~100; methyl orange: ~100	95
rGO/MXene hybrid hydrogel	Modified Hummers' method + chemical reduction + directional-freezing + thawing	2.09	94	Na^+: ~99; Mg^{2+}: ~99; K^+: ~99; Ca^{2+}: ~99; B^{3+}: ~98	96
MXene/GO/PANI hybrid	Mechanical mixing + self-assembly Intercalation + directional-freezing	3.94	136	K^+: ~99.9; Ca^{2+}: ~99.9; Cr^{3+}: ~99.9; Cu^{2+}: ~99.9; Pb^{2+}: ~99.9; Zn^{2+}: ~99.9	97
rGO/HNs	Solvothermal treatment + ultrasonication + mechanical stirring + vacuum filtration + thermal reduction	1.48	89	Pb^{2+}: 99.9; Ni^{2+}: 99.9; Al^{3+}: 99.9	98

this membrane exhibited a higher PTCE of 86% with a corresponding water evaporation rate of 1.37 kg m^{-2} h^{-1} at one-sun illumination. This work also investigates the effect on the mass loadings of rGO towards solar absorption capabilities and an increase in the evaporation mass of water, suggesting the suitability of rGO in photothermal conversion. In another work, Zhou *et al.*[87] reported the synthesis of unique one-dimensional graphene fibers (GFs). Firstly, $MgCO_3$ fibers were produced by the precipitation method then annealed at 850 °C under an Ar atmosphere to obtain porous MgO fibers. Subsequently, ethanol aerosol was introduced into the foaming carrier gas for the growth of graphitic carbon on the MgO fiber template. Lastly, the template was removed using HCl and the as-obtained GFs were filtered onto cellulose fiber paper *via* vacuum filtration, resulting in the formation of a Janus membrane, as shown in Fig. 4a. The N_2 adsorption/desorption graph (Fig. 4b) revealed that GFs contain numerous mesopores between 2 and 30 nm that allow incident light to be absorbed directly and then enable multiple reflections within the porous structure, as shown in the inset of Fig. 4b. As a result, it leads to an enhancement in the light harvesting property. Under different solar intensities, the mass loss of water increases similarly signifying that the GF-based Janus evaporator works effectively to evaporate water (Fig. 4c). As such, this fabricated GF-based Janus membrane showed an excellent water evaporation rate of 1.40 kg m^{-2} h^{-1} with a PTCE of 88%. Such a superb performance can also be attributed to the interconnected network structure which improves the vapor transport capabilities. The top surface of the GFs/cellulose membrane revealed that the stacked GF layer has a porous network structure made of interconnected GFs, whereas the bottom surface showed that the cellulose fiber paper is porous. These porous network structures provide numerous pathways for water vapor transportation. Also, it has been demonstrated that the as-fabricated membrane has robust stability that can withstand bending. It is also worth noting that the salt rejection of this photothermal membrane was estimated to be 99.9% for Cu^{2+}, Mn^{2+} and Cd^{2+} ions,

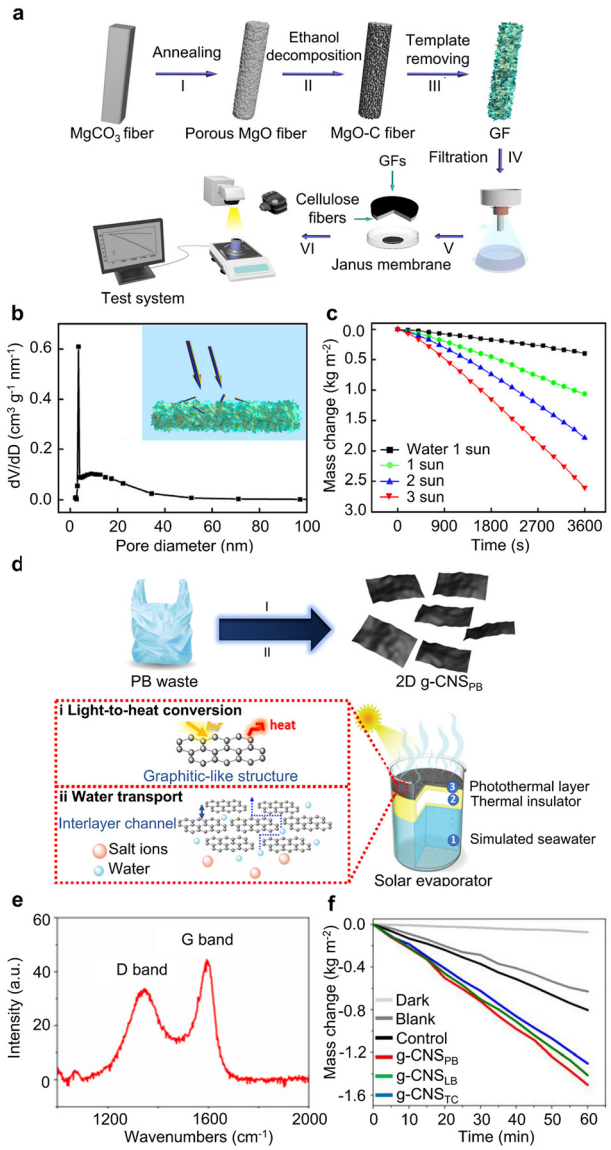

Fig. 4 (a) Schematic illustration of the fabrication of GF-based Janus membrane evaporator. (b) N_2 adsorption and desorption curve and the schematic illustration of light absorption and reflection in the inset. (c) Mass change of water against varying solar intensities.[87] These figures have been adapted from ref. 87 with permission from Elsevier, Copyright 2021. (d) Schematic illustration of 2D graphitic carbon nanosheets from plastic waste polymers. (e) Raman spectrum and (f) cumulative mass change of various samples under one-sun solar illumination.[91] These figures have been adapted from ref. 91 with permission from Elsevier, Copyright 2021.

respectively. These divalent ion rejection percentages are much higher compared to the ones in NF. To enhance the water evaporation rate, Aizudin *et al.*[99] reported a sustainable facile two-step solvothermal method followed by carbonization to convert plastic waste polymers into graphitic carbon nanosheets that possess both excellent light-to-heat conversion and well-organized interlayer channel properties (Fig. 4d). The latter is further verified in Raman measurements which revealed that the 2D g-CNS_{PB} sample showed a higher intensity ratio of G and D bands (I_G/I_D) indicating a higher degree of structural ordering for graphite which enables fast water transportation, as depicted in Fig. 4e. As such, this accounts for the high evaporation rate of 1.50 kg m^{-2} h^{-1} with a PTCE of 99%, as shown in Fig. 4f. In another work, Wang *et al.*[88] utilized a porous textile denoted as blank hollow spacer fabric (BHSF) as support and filled it up with chitosan for uniform coating of GO followed by chemical reduction into rGO onto chitosan-modified BHSF using hydrazine hydrate. The unique hollow structure of BHSF, with an aligned large channel array (2 mm in size), which supplied extra low-tortuosity pathways for water evaporation and the rGO/chitosan modified BHSF provide exceptional salt-resistance capabilities (>99.9% rejection for K^+, Ca^{2+}, Na^+ and Mg^{2+}), even in concentrated saline solution (*i.e.*, 382 to 10 474 mg L^{-1}). Recently, the porous three-dimensional (3D) graphene-based network structure has attracted much attention in SD due to its attractive properties like low density, high porosity and potential photothermal materials.[100] For example, Li *et al.*[89] designed a 3D network structure containing rGO and cellulose nanocrystal (CNC) lamella network (rGO-CNC) on melamine foam (MF), which served as a template, by a squeezing immersion method to embed GO and CNC into MF. Due to the superb light absorption properties of rGO and excellent hydrophilic properties of CNCs, the rGO-CNC/MA photothermal membrane displayed an evaporation rate of 1.66 kg m^{-2} h^{-1} with PTCE of 98%. Moreover, when subjected to harsh conditions and long-term durability tests (over 20 days, 120 min per day), the rGO-CNC/MF photothermal membrane still displayed excellent structural stability and water evaporation performances. In another similar work, Chen *et al.*[90] synthesized a 3D network structure of rGO on a poly(*p*-phenylene benzobisoxazole) nanofiber (PBONF) aerogel *via* simple molding in combination with freeze drying. The as obtained rGO/PBONF comprises a 3D porous framework that is interconnected with PBONF fibers and rGO nanosheets. Such a unique structure has multiple channels for fast water vapor transportation, leading to fast mass change of water per unit time, resulting in a water evaporation rate of 1.74 kg m^{-2} h^{-1} with an excellent PTCE of 98% thanks to the broadband wavelength absorption from 300–2500 nm. In this work, the use of CF is advantageous for water transportation due to its inherent super hydrophilic nature, as verified by the contact angle measurement. This favorable characteristic coupled with the near 100% broad light absorption of rGO materials can deliver a high-water evaporation rate of 1.62 kg m^{-2} h^{-1} with a relatively high PTCE of 94% under one-sun illumination. Among all the recent reported values for PTCE and water evaporation rates (see Table 3), Li *et al.*[93] has demonstrated that the vertically aligned rGO (V-rGO) foam obtained from freeze drying followed by chemical reduction, has an extremely high water evaporation rate of 3.39 kg m^{-2} h^{-1} and superior PTCE at 104%. Interestingly, this work utilizes a dynamic compression strategy in tuning the energy state of water in the pore channels of V-rGO foam. For instance, by optimal dynamic compression, the vaporization enthalpy of water significantly decreases due

to the increased proportion of intermediate water thus leading to a higher water evaporation rate.

Chemically doped graphene-based membranes

As is well known, doping can affect the hydrophilicity of GBnMs, with nitrogen dopants being a popular choice due to their comparable atomic size and the presence of valence electrons that can form strong bonds with carbon atoms.[37] This is a useful property because it allows for the rapid transport of water molecules.[38] For nitrogen doping, Deng *et al.*[38] added ethylenediamine (EDA) as the nitrogen source into the GO solution and performed hydrothermal treatment followed by freeze drying to obtain a N-doped rGO aerogel. Lastly, various annealing temperatures (200–1000 °C) were investigated on the hydrophilicity property of the N-doped rGO aerogel. The unique superwetting performance of the N-doped rGO aerogel over pristine rGO arises from the synergy of nitrogen doping and the thermal annealing process, as evidenced by the contact angle measurements. It was observed that at a high annealing temperature, the N-doped rGO aerogel became more hydrophobic because more oxygen-containing functional groups were removed from the rGO. The presence of the water molecule layer increases the van der Waals interaction distance between the rGO layers and the airborne hydrocarbon, significantly inhibiting the hydrocarbon adsorption rate, resulting in an unusually long-term superwetting behaviour, which promotes fast water evaporation rate of 1.41 kg m^{-2} h^{-1}. In a similar work, Huo *et al.*[39] have fabricated a N-doped rGO aerogel using melamine form (MF) as the nitrogen dopant source. Through dip-coating GO onto MF foam followed by air-drying and thermal treatment, the 3D N-doped rGO aerogel was obtained. The MF also served as a skeleton template for the formation of an interconnected 3D network structure with micrometer-sized pores. The abundance of micropores enables water vapor to escape, leading to a higher evaporation rate of 1.56 kg m^{-2} h^{-1}. The excellent solar light absorption of the 3D N-doped rGO aerogel is estimated to be 97.6% and this accounts for the high PTCE of 90%. In addition, the high specific surface area (517.24 m^2 g^{-1}) of the 3D N-doped rGO aerogel can also be the reason for its efficient light absorption. Moreover, when compared to the undoped pristine GO, the high intensity D band under Raman spectra analysis of the N-doped rGO sample revealed that after N doping, the formation of lattice defects can result in lower thermal conductivity, which greatly enhances heat trapping, and thus boosts the PTCE of the materials. Allahbakhsh *et al.*[37] have used a facile approach to synthesize N-doped graphene quantum dots (N-GQDs) by simply performing a hydrothermal treatment on PEI solution. Then L-ascorbic acid was used for the self-assembly and reduction of the N-GQDs into a hydrogel network, which was used for solar evaporation. The resultant photothermal layer exhibited a high PTCE of 90% with a water evaporation rate of 1.4 kg m^{-2} h^{-1}. The prepared N-GQD hydrogels have high SD performances due to their hierarchical pore structure, high hydrophilicity, and low thermal conductivity.

Graphene-based composite membranes

When compared to its pristine form, the integration of graphene derivatives and other emerging materials (such as inorganic materials, MXene, g-C_3N_4, *etc.*) commonly has a synergistic effect on both the rate of water evaporation and the extent of PTCE. The g-C_3N_4 materials are known for their strong absorption in the visible light region and photocatalytic degradation.[101] Recently, Su *et al.*[94] have fabricated a g-C_3N_4/GO hybrid hydrogel by simply mixing g-C_3N_4 and GO together followed by hydrothermal treatment. The resultant g-C_3N_4/GO hybrid hydrogel due to the extensively porous design and wide light absorption exhibited a high-water evaporation rate of 1.09 kg m^{-2} h^{-1} with PTCE of 75%. Interestingly, Ren *et al.*[95] reported the fabrication of 3D carbonized loofah sponges (CLS) embedded with Cu nanoparticles coated with graphene shell (Cu@G) using hydrothermal treatment to integrate Cu-MOF into the natural loofah followed by pyrolysis to carbonize the organic linkers into graphitic materials, as depicted in Fig. 5a. In addition to the 3D porous and elongated microchannels of CLS, the Cu@G/CLS hybrid also possessed a high surface temperature of 72 °C due to the localized heating effect of stabilized Cu nanoparticles under simulated solar illumination. Such efficient localized heating can be attributed to the presence of graphene that protects Cu from undergoing oxidation under ambient conditions as evidenced from the absence of satellite peaks in the Cu 2p spectrum of Cu@G/CLS (Fig. 5b). These resulted in high-water mass change per unit time of Cu@G/CLS (Fig. 5c) when compared to that in pristine CLS, leading to a water evaporation rate of 1.54 kg m^{-2} h^{-1} with a corresponding PTCE of 90% at one-sun solar illumination. To investigate the efficacy of the water purification of Cu@G/CLS, MB and MO probe solutes were used, while the UV-vis measurements of before and after SD showed both the rejection rates were near 100%. MXene has excellent light absorption and high light-to-heat conversion efficiency, making it attractive towards SD.[102] For instance, Li *et al.*[96] engineered a photothermal hydrogel based on rGO/MXene hybrid through chemical reduction of GO using ascorbic acid into a rGO hydrogel then using the Marangoni effect for solvent exchange to intercalate the MXene sheets into the rGO hydrogel followed by directional freezing and thawing, producing a vertically aligned rGO/MXene hybrid hydrogel, which achieves a higher water evaporation rate of 2.09 kg m^{-2} h^{-1} as compared to that of pristine rGO (1.8 kg m^{-2} h^{-1}), indicating the synergistic effect of the rGO/MXene composite. In another similar work, the as-prepared GO and MXene were mixed homogeneously in a solution containing polyaniline (PANI).[97] The presence of PANI facilitates electrostatic self-assembly of the intercalated GO/MXene/GO/MXene layered structure and formed aggregates, which can be easily reshaped into a cylindrical mold for directional freezing. Due to its low water vaporization enthalpy and excellent solar-thermal energy conversion of hydrophilic GO/MXene/PANI hybrid, the resultant cylindrical MXene/GO/PANI exhibited an outstanding water evaporation rate of 3.94 kg m^{-2} h^{-1} with an extremely high PTCE of

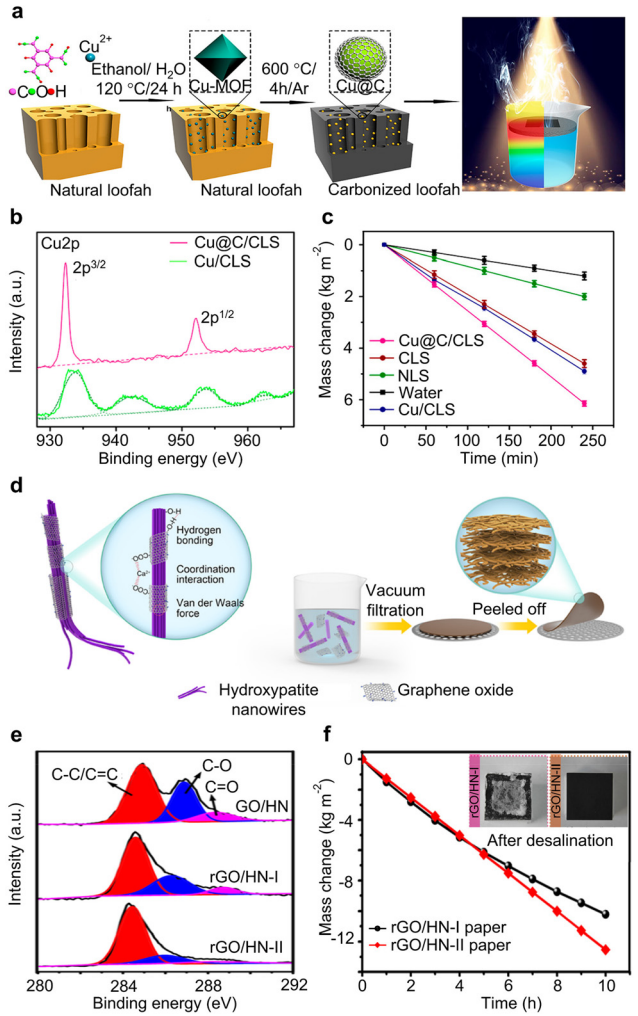

Fig. 5 (a) Schematic illustration for the synthesis of a Cu@G/CLS structure. (b) XPS Cu 2p spectra of Cu@C/CLS and Cu/CLS. (c) Water evaporation performance of Cu@G/CLS solar evaporator *versus* other samples under one sun illumination.[95] These figures have been adapted from ref. 95 with permission from American Chemical Society, Copyright 2021. (d) Hierarchical assembly of GO and HNs and the schematic illustration of GO/HN paper with a layered structure *via* a vacuum-assisted filtration process. (e) XPS patterns of GO/HN, rGO/HN-I and rGO/HN-II. (f) Mass change of SD performance of rGO/HN-I paper and rGO/HN-II paper with the digital images after desalination.[98] These figures have been adapted from ref. 98 with permission from American Chemical Society, Copyright 2020.

136%, which is so far among the best reported performances from the literature. To obtain an interconnected network structure in a photothermal membrane, which can be directly used for SD, Xiong *et al.*[98] synthesized ultralong hydroxyapatite nanowires (HNs) through solvothermal treatment and then mixed with glass fiber and GO *via* mechanical stirring before vacuum filtration to form a GO/HN membrane that was cross-linked *via* hydrogen bonding, coordination interaction and van der Waals forces of attraction (Fig. 5d). Next, the membrane was thermally treated at 150 °C under vacuum to obtain a rGO/HN composite. The as-fabricated rGO/HN composite membrane consists of a hierarchical porous structure with interconnected channels and wide solar light absorption that led to a high evaporation rate of 1.48 kg m^{-2} h^{-1} and PTCE of 90%. Notably, the hydrophilicity and hydrophobicity of the rGO/HN photothermal layer can be modified by controlling the thermal treatment time for 2 h and 6 h, respectively. Upon thermal treatment, the peak intensities of oxygen-containing groups (C–O and C═O) decrease in the XPS C 1s spectrum of the hydrophilic rGO/HN-I and hydrophobic rGO/HN-II (see Fig. 5e). This advantageous property can be beneficial especially for salt-rejection performance in seawater desalination applications. As expected, the mass change of rGO/HN-I is reported to be less linear than that of rGO/HN-II due to the accumulation of salt crystals on the hydrophilic layer that blocks the pores for water transportation (see Fig. 5f and inset Fig. 5f). Moreover, the flexible rGO/HN photothermal membrane can also produce clean water from seawater with high rejection rates of metal ions, which meet the drinking quality stated by the World Health Organization (WHO) and US Environmental Protection Agency (EPA).

Conclusions and future outlook

In this mini-review, we presented the recent progress of GBnM membranes consisting of graphene derivatives, chemically doped graphene, and graphene-based composites in NF and SD applications. Here, GBnMs can function as building blocks of membrane fabrication with controllable selective layer thickness and adjustable interlayer channels, which are very important in optimizing the NF performances of the membrane technology for water treatment. Furthermore, the wide solar absorption bandwidth of GBnMs provides excellent solar-to-heat conversion efficiency of the photothermal evaporator for an enhanced SD process. Based on their synthesis methods, materials combinations, and corresponding application performances, the creation of innovative and functional materials has significantly enabled the collaborative advancement of various fields of studies.

However, the majority of GBnM membrane studies continue to use commercial graphite, and the rising demand for GBnMs has undoubtedly had a detrimental social impact on the mining of natural graphite resources. As a result, alternative technologies such as waste recycling to generate graphitic-like structures are required.[84] This allows for the reduction of feedstock costs as well as the provision of alternative sustainable materials. The preparation of GBnM membranes in water treatment is still restricted by the fabrication techniques such as drop-casting, surface coating, and vacuum filtration, and their performances are frequently limited due to structural design and controllable dimension constraints; besides multiple steps are required for fabricating a single structure from multiple components. Therefore, an easy operating strategy, with a universal, low-cost, and automated system, for instance, additive manufacturing, is needed to accelerate the process of prototyping. Incorporating experimentation with theoretical

computation of GBnMs provides a powerful stimulus for experimentation while also leading to excellence in scientific implications. Moreover, computational simulation methods can also provide guidance for new material application prediction. We envisage that this mini-review will provide a summary of recent previous work to advance the development of GBnMs in the water purification technology sector.

Conflicts of interest

There are no conflicts to declare.

Acknowledgements

E. H. A. thanks the Ministry of Education, Singapore, under its Academic Research Fund Tier 1 (RG10/22), National Research Foundation, Singapore (NRF-MP-2022-0001), National Institution of Education Start Up Grant (NIE-SUG4/20AHX) and NIE-AcRF Grant (RI 1/21 EAH) for their funding support.

References

1 S. Yadav, H. Saleem, I. Ibrar, O. Naji, A. A. Hawari, A. A. Alanezi, S. J. Zaidi, A. Altaee and J. Zhou, *Desalination*, 2020, **482**, 114375.
2 K. Wang, X. Wang, B. Januszewski, Y. Liu, D. Li, R. Fu, M. Elimelech and X. Huang, *Chem. Soc. Rev.*, 2022, **51**, 672–719.
3 T. M. Zewdie, N. G. Habtu, A. Dutta and B. Van der Bruggen, *J. Water Reuse Desalin.*, 2020, **11**, 1–32.
4 Z. Wang, X. Wu, J. Dong, X. Yang, F. He, S. Peng and Y. Li, *J. Chem. Eng.*, 2022, **427**, 130905.
5 K. Xu, C. Wang, Z. Li, S. Wu and J. Wang, *Adv. Funct. Mater.*, 2021, **31**, 2007855.
6 X. Han, L. V. Besteiro, C. S. L. Koh, H. K. Lee, I. Y. Phang, G. C. Phan-Quang, J. Y. Ng, H. Y. F. Sim, C. L. Lay, A. Govorov and X. Y. Ling, *Adv. Funct. Mater.*, 2021, **31**, 2008904.
7 E. H. Ang and J. W. Chew, *Chem. Mater.*, 2019, **31**, 10002–10007.
8 E. H. Ang, S. Velioğlu and J. W. Chew, *J. Membr. Sci.*, 2019, **591**, 117318.
9 X. Lin, M. Yang, W. Hong, D. Yu and X. Chen, *Front. Mater.*, 2018, **5**, 74.
10 A. Stergiou, R. Cantón-Vitoria, M. N. Psarrou, S. P. Economopoulos and N. Tagmatarchis, *Prog. Mater. Sci.*, 2020, **114**, 100683.
11 A. G. Olabi, M. A. Abdelkareem, T. Wilberforce and E. T. Sayed, *Renewable Sustainable Energy Rev.*, 2021, **135**, 110026.
12 C. Anichini and P. Samorì, *Small*, 2021, **17**, 2100514.
13 D. Hou, S. Zhang, X. Chen, R. Song, D. Zhang, A. Yao, J. Sun, W. Wang, L. Sun, B. Chen, Z. Liu and L. Wang, *ACS Appl. Mater. Interfaces*, 2021, **13**, 10328–10335.
14 C. Cheng, Q. Liang, M. Yan, Z. Liu, Q. He, T. Wu, S. Luo, Y. Pan, C. Zhao and Y. Liu, *J. Hazard. Mater.*, 2022, **424**, 127721.
15 C. Bie, H. Yu, B. Cheng, W. Ho, J. Fan and J. Yu, *Adv. Mater.*, 2021, **33**, 2003521.
16 H. Wu, S. Deng, Y. Shao, J. Yang, X. Qi and Y. Wang, *ACS Appl. Mater. Interfaces*, 2019, **11**, 46851–46863.
17 T. Yan, T. Li, J. Xu, J. Chao, R. Wang, Y. I. Aristov, L. G. Gordeeva, P. Dutta and S. S. Murthy, *ACS Energy Lett.*, 2021, **6**, 1795–1802.
18 D.-Z. Chen, S.-Y. Qin, G. C. P. Tsui, C.-y. Tang, X. Ouyang, J.-h. Liu, J.-N. Tang and J.-D. Zuo, *Composites, Part B*, 2019, **157**, 239–247.
19 A. Olabi, M. A. Abdelkareem, T. Wilberforce and E. T. Sayed, *Renewable Sustainable Energy Rev.*, 2021, **135**, 110026.
20 T. Tite, E. A. Chiticaru, J. S. Burns and M. Ioniță, *J. Nanobiotechnol.*, 2019, **17**, 101 (2019).
21 F. Esposito, L. Sansone, A. Srivastava, F. Baldini, S. Campopiano, F. Chiavaioli, M. Giordano, A. Giannetti and A. Iadicicco, *Biosens. Bioelectron.*, 2021, **172**, 112747.
22 J. Yoon, J. Lim, M. Shin, S.-N. Lee and J.-W. Choi, *Materials*, 2021, **14**, 518.
23 C. Chen, Y. Kuang and L. Hu, *Joule*, 2019, **3**, 683–718.
24 P. Das and S. Dutta, in *Membranes with Functionalized Nanomaterials*, ed. S. Dutta and C. M. Hussain, Elsevier, 2022, pp. 159–183.
25 Y. Vasseghian, E.-N. Dragoi, F. Almomani, V. T. Le and M. Berkani, *Environ. Technol. Innovation*, 2021, **24**, 101863.
26 Y. Li, S. Yuan, Y. Xia, W. Zhao, C. D. Easton, C. Selomulya and X. Zhang, *J. Membr. Sci.*, 2020, **601**, 117900.
27 F. J. García-Picazo, S. Pérez-Sicairos, G. A. Fimbres-Weihs, S. W. Lin, M. I. Salazar-Gastélum and B. Trujillo-Navarrete, *Polymer*, 2021, **13**, 1637.
28 A. T. N. Azam Marjani, M. Adimi, H. F. Jirandehi and S. Shirazian, *Sci. Rep.*, 2020, **10**, 2049.
29 C. P. Athanasekou, M. F. Pedrosa, A. M. T. Silva, V. P. Psycharis and G. E. Romanos, *Adv. Chem. Eng.*, 2021, **5**, 100066.
30 C. M. Bezerra de Araujo, G. Filipe Oliveira do Nascimento, G. Rodrigues Bezerra da Costa, K. Santos da Silva, A. M. Salgueiro Baptisttella, M. Gomes Ghislandi and M. Alves da Motta Sobrinho, *Chem. Eng. Commun.*, 2019, **206**, 1375–1387.
31 S. A. Alkahtani, A. M. Mahmoud, M. H. Mahnashi, R. Ali and M. M. El-Wekil, *Biosens. Bioelectron.*, 2021, **183**, 113202.
32 W. Wang, J. Jin, Y. Wu, W. Zhang, H. Jiang, X. Li and G. Wang, *J. Mater. Chem. A*, 2019, **7**, 22054–22062.
33 A. Reheman, K. Kadeer, K. Okitsu, M. Halidan, Y. Tursun, T. Dilinuer and A. Abulikemu, *Ultrason. Sonochem.*, 2019, **51**, 166–177.
34 P. Zhang, J.-L. Gong, G.-M. Zeng, B. Song, S. Fang, M. Zhang, H.-Y. Liu, S.-Y. Huan, P. Peng, Q.-Y. Niu, D.-B. Wang and J. Ye, *Sep. Purif. Technol.*, 2019, **220**, 309–319.

35 G. Cheng, X. Wang, X. Liu, Y. He and B. V. Balakin, *Sol. Energy*, 2019, **194**, 415–430.
36 R. Hou, Y. He, H. Yu, J. Ma, Y. Gao, Y. Bai and J. Chen, *Chem. Phys. Lett.*, 2021, **775**, 138657.
37 A. Allahbakhsh, *Desalination*, 2021, **517**, 115264.
38 X. Deng, Q. Nie, Y. Wu, H. Fang, P. Zhang and Y. Xie, *ACS Appl. Mater. Interfaces*, 2020, **12**, 26200–26212.
39 B. Huo, D. Jiang, X. Cao, H. Liang, Z. Liu, C. Li and J. Liu, *Carbon*, 2019, **142**, 13–19.
40 D. Yang, B. Xu, Q. Zhao and X. S. Zhao, *J. Mater. Chem. A*, 2019, **7**, 363–371.
41 Y. Yu, J. Zheng, J. Li, L. Lu, J. Yan, L. Zhang and L. Wang, *Trends Food Sci. Technol.*, 2021, **110**, 443–457.
42 X. Hu, Z. Hemmat, L. Majidi, J. Cavin, R. Mishra, A. Salehi-Khojin, S. Ogut and R. F. Klie, *Small*, 2020, **16**, 1905892.
43 D. K. Lee, S. J. Kim, Y.-J. Kim, H. Choi, D. W. Kim, H.-J. Jeon, C. W. Ahn, J. W. Lee and H.-T. Jung, *Adv. Mater. Interfaces*, 2019, **6**, 1801992.
44 L. Yan, Y. Xu, P. Chen, S. Zhang, H. Jiang, L. Yang, Y. Wang, L. Zhang, J. Shen, X. Zhao and L. Wang, *Adv. Mater.*, 2020, **32**, 2003313.
45 R. Fang, K. Chen, L. Yin, Z. Sun, F. Li and H.-M. Cheng, *Adv. Mater.*, 2019, **31**, 1800863.
46 Y. Xu, P. Deng, G. Chen, J. Chen, Y. Yan, K. Qi, H. Liu and B. Y. Xia, *Adv. Funct. Mater.*, 2020, **30**, 1906081.
47 X. Sun, C. Huang, L. Wang, L. Liang, Y. Cheng, W. Fei and Y. Li, *Adv. Mater.*, 2021, **33**, 2001105.
48 V. Gund, A. Ruyack, A. Leonardi, K. B. Vinayakumar, C. Ober and A. Lal, *Adv. Funct. Mater.*, 2019, **29**, 1900592.
49 A. U. Khan, G. Zeltzer, G. Speyer, Z. L. Croft, Y. Guo, Y. Nagar, V. Artel, A. Levi, C. Stern, D. Naveh and G. Liu, *Adv. Mater.*, 2021, **33**, 2004053.
50 N. M. Mahmoodi and M. H. Saffar-Dastgerdi, *Appl. Catal., B*, 2020, **268**, 118443.
51 N. S. Kim, M. Oh, K. Kim and C. Jo, *J. Chem. Eng.*, 2021, **409**, 128076.
52 J. Li, C. Xu, J. Long, Z. Ding, R. Yuan and Z. Li, *ACS Appl. Nano Mater.*, 2022, **5**, 7373–7381.
53 H. Ang and L. Hong, *ACS Appl. Mater. Interfaces*, 2017, **9**, 28079–28088.
54 H. Ang and L. Hong, *J. Mater. Chem. A*, 2017, **5**, 20598–20602.
55 A. O. E. Abdelhalim, A. A. Meshcheriakov, D. N. Maistrenko, O. E. Molchanov, S. V. Ageev, D. A. Ivanova, N. R. Iamalova, M. D. Luttsev, L. V. Vasina, V. V. Sharoyko and K. N. Semenov, *Colloids Surf., B*, 2022, **210**, 112232.
56 L. Yang, X. Xiao, S. Shen, J. Lama, M. Hu, F. Jia, Z. Han, H. Qu, L. Huang, Y. Wang, T. Wang, Z. Ye, Z. Zhu, J. Tang and J. Chen, *ACS Appl. Nano Mater.*, 2022, **5**, 3121–3145.
57 A. Marjani, A. T. Nakhjiri, M. Adimi, H. F. Jirandehi and S. Shirazian, *Sci. Rep.*, 2020, **10**, 2049.
58 J. Li, M. Hu, H. Pei, X. Ma, F. Yan, D. S. Dlamini, Z. Cui, B. He, J. Li and H. Matsuyama, *J. Membr. Sci.*, 2020, **595**, 117547.
59 A. Iakunkov, N. Boulanger, A. Nordenström and A. V. Talyzin, *Adv. Mater. Interfaces*, 2021, **8**, 2100552.
60 Z. Zhao, S. Ni, X. Su, Y. Gao and X. Sun, *ACS Sustainable Chem. Eng.*, 2019, **7**, 14874–14882.
61 X. Fan, C. Cai, J. Gao, X. Han and J. Li, *Sep. Purif. Technol.*, 2020, **241**, 116730.
62 J. M. Luque-Alled, A. Abdel-Karim, M. Alberto, S. Leaper, M. Perez-Page, K. Huang, A. Vijayaraghavan, A. S. El-Kalliny, S. M. Holmes and P. Gorgojo, *Sep. Purif. Technol.*, 2020, **230**, 115836.
63 C. Xing, J. Han, X. Pei, Y. Zhang, J. He, R. Huang, S. Li, C. Liu, C. Lai, L. Shen, A. K. Nanjundan and S. Zhang, *ACS Appl. Mater. Interfaces*, 2021, **13**, 55339–55348.
64 M. H. Jian Li, H. Pei, X. Ma, F. Yan, D. S. Dlamini, Z. Cui, B. He, J. Li and H. Matsuyama, *J. Membr. Sci.*, 2020, **595**, 117547.
65 A. A.-K. Jose Miguel Luque-Alleda, M. Alberto, S. Leaper, M. Perez-Page, K. Huang, A. Vijayaraghavan, A. S. El-Kalliny, S. M. Holmes and P. Gorgojo, *Sep. Purif. Technol.*, 2020, **230**, 115836.
66 J. H. Chao Xing, X. Pei, Y. Zhang, J. He, R. Huang, S. Li, C. Liu, C. Lai, L. Shen, A. K. Nanjundan and S. Zhang, *ACS Appl. Mater. Interfaces*, 2021, **13**, 55339–55348.
67 Z. Liu, Z. Ma, B. Qian, A. Y. H. Chan, X. Wang, Y. Liu and J. H. Xin, *ACS Nano*, 2021, **15**, 15294–15305.
68 G. Zhao, R. Hu, Y. He and H. Zhu, *Adv. Mater. Interfaces*, 2019, **6**, 1801742.
69 K. M. Cho, H.-J. Lee, Y. T. Nam, Y.-J. Kim, C. Kim, K. M. Kang, C. A. Ruiz Torres, D. W. Kim and H.-T. Jung, *ACS Appl. Mater. Interfaces*, 2019, **11**, 27004–27010.
70 M. Zhang, K. Guan, Y. Ji, G. Liu, W. Jin and N. Xu, *Nat. Commun.*, 2019, **10**, 1253.
71 M. Zhang, Y. Mao, G. Liu, G. Liu, Y. Fan and W. Jin, *Angew. Chem., Int. Ed.*, 2020, **59**, 1689–1695.
72 Q. Huang, S. Liu, Y. Guo, G. Liu and W. Jin, *J. Membr. Sci.*, 2022, **645**, 120212.
73 W.-H. Zhang, M.-J. Yin, Q. Zhao, C.-G. Jin, N. Wang, S. Ji, C. L. Ritt, M. Elimelech and Q.-F. An, *Nat. Nanotechnol.*, 2021, **16**, 337–343.
74 H. Qu, X. Xiao, Z. Han, M. Hu, S. Shen, L. Yang, F. Jia, T. Wang, Z. Ye, W. Sun, Y. Wang, L. Huang, Z. Zhu, P. Servati, J. Tang and J. Chen, *ACS Appl. Nano Mater.*, 2022, **5**, 5196–5207.
75 Q. Liu, N. Basel, L. Li, N. Xu, Q. Dong, L. Fan, Q. Wang, A. Ding and T. Wang, *J. Membr. Sci.*, 2022, **647**, 120296.
76 X. Sui, Z. Yuan, C. Liu, L. Wei, M. Xu, F. Liu, A. Montoya, K. Goh and Y. Chen, *J. Mater. Chem. A*, 2020, **8**, 9713–9725.
77 H. Deng, Q. Zheng, H. Chen, J. Huang, H. Yan, M. Ma, M. Xia, K. Pei, H. Ni and P. Ye, *Sep. Purif. Technol.*, 2021, **278**, 119440.
78 X. Zhao, Y. Che, Y. Mo, W. Huang and C. Wang, *J. Membr. Sci.*, 2021, **640**, 119847.
79 J.-J. Lu, Y.-H. Gu, Y. Chen, X. Yan, Y.-J. Guo and W.-Z. Lang, *Sep. Purif. Technol.*, 2019, **210**, 737–745.
80 Q. Huang, S. Liu, Y. Guo, G. Liu and W. Jin, *J. Membr. Sci.*, 2022, **645**, 120212.

81 M. Zhang, Y. Mao, G. Liu, G. Liu, Y. Fan and W. Jin, *Angew. Chem.*, 2019, **132**, 1706–1712.
82 M. Zhang, K. Guan, Y. Ji, G. Liu, W. Jin and N. Xu, *Nat. Commun.*, 2019, **10**, 1253.
83 L. Wu, Z. Dong, Z. Cai, T. Ganapathy, N. X. Fang, C. Li, C. Yu, Y. Zhang and Y. Song, *Nat. Commun.*, 2020, **11**, 521.
84 M. Aizudin, R. Goei, A. J. Ong, Y. Z. Tan, S. K. Lua, R. Poolamuri Pottammel, H. Geng, X.-L. Wu, A. L. Yoong Tok and E. H. Ang, *J. Mater. Chem. A*, 2022, **10**, 19612–19617.
85 D.-D. Han, Z.-D. Chen, J.-C. Li, J.-W. Mao, Z.-Z. Jiao, W. Wang, W. Zhang, Y.-L. Zhang and H.-B. Sun, *ACS Appl. Mater. Interfaces*, 2020, **12**, 25435–25443.
86 W. Chen, P. Xiao, H. Chen, H. Zhang, Q. Zhang and Y. Chen, *Adv. Mater.*, 2019, **31**, 1802403.
87 Q. Zhou, H. Li, D. Li, B. Wang, H. Wang, J. Bai, S. Ma and G. Wang, *J. Colloid Interface Sci.*, 2021, **592**, 77–86.
88 F. Wang, D. Wei, Y. Li, T. Chen, P. Mu, H. Sun, Z. Zhu, W. Liang and A. Li, *J. Mater. Chem. A*, 2019, **7**, 18311–18317.
89 H. Li, D. Jia, M. Ding, L. Zhou, K. Wang, J. Liu, C.-Y. Liu and C. Li, *Sol. RRL*, 2021, **5**, 2100317.
90 M. Chen, X. Lin, C. Zeng and Q. He, *Colloids Surf., A*, 2021, **612**, 125997.
91 M. Aizudin, R. Goei, A. J. Ong, Y. Z. Tan, S. K. Lua, R. Poolamuri Pottammel, H. Geng, X.-L. Wu, A. L. Yoong Tok and E. H. Ang, *J. Mater. Chem. A*, 2022, **10**, 19612–19617.
92 H. Sun, Y. Li, Z. Zhu, P. Mu, F. Wang, W. Liang, C. Ma and A. Li, *ChemSusChem*, 2019, **12**, 4257–4264.
93 W. Li, X. Tian, X. Li, S. Han, C. Li, X.-Z. Zhai, Y. Kang and Z.-Z. Yu, *J. Mater. Chem. A*, 2021, **9**, 14859–14867.
94 H. Su, J. Zhou, L. Miao, J. Shi, Y. Gu, P. Wang, Y. Tian, X. Mu, A. Wei, L. Huang, S. Chen and Z. Deng, *Sustainable Mater. Technol.*, 2019, **20**, e00095.
95 L. Ren, X. Yi, Z. Yang, D. Wang, L. Liu and J. Ye, *Nano Lett.*, 2021, **21**, 1709–1715.
96 W. Li, X. Li, W. Chang, J. Wu, P. Liu, J. Wang, X. Yao and Z.-Z. Yu, *Nano Res.*, 2020, **13**, 3048–3056.
97 X.-P. Li, X. Li, H. Li, Y. Zhao, J. Wu, S. Yan and Z.-Z. Yu, *Adv. Funct. Mater.*, 2022, **32**, 2110636.
98 Z.-C. Xiong, Y.-J. Zhu, D.-D. Qin and R.-L. Yang, *ACS Appl. Mater. Interfaces*, 2020, **12**, 32556–32565.
99 M. Aizudin, R. Goei, A. J. Ong, Y. Z. Tan, S. K. Lua, R. Poolamuri Pottammel, H. Geng, X.-L. Wu, A. L. Yoong Tok and E. H. Ang, *J. Mater. Chem. A*, 2022, **10**, 19612–19617.
100 C. T. K. Finnerty, A. K. Menon, K. M. Conway, D. Lee, M. Nelson, J. J. Urban, D. Sedlak and B. Mi, *Environ. Sci. Technol.*, 2021, **55**, 15435–15445.
101 H. Wang, Y. Wu, M. Feng, W. Tu, T. Xiao, T. Xiong, H. Ang, X. Yuan and J. W. Chew, *Water Res.*, 2018, **144**, 215–225.
102 X. Zhao, X.-J. Zha, J.-H. Pu, L. Bai, R.-Y. Bao, Z.-Y. Liu, M.-B. Yang and W. Yang, *J. Mater. Chem. A*, 2019, **7**, 10446–10455.